Ultrasound in Med. & Biol., Vol. 42, No. 6, pp. 1375–1384, 2016
Copyright © 2016 World Federation for Ultrasound in Medicine & Biology
Printed in the USA. All rights reserved
0301-5629/$ - see front matter

http://dx.doi.org/10.1016/j.ultrasmedbio.2016.01.018

● *Original Contribution*

SPECIES-INDEPENDENT MODELING OF HIGH-FREQUENCY ULTRASOUND BACKSCATTER IN HYALINE CARTILAGE

Nils Männicke,* Martin Schöne,* Jukka Liukkonen,† Dominik Fachet,‡ Satu Inkinen,† Markus K. Malo,† Michael L. Oelze,§ Juha Töyräs,†¶ Jukka S. Jurvelin,† and Kay Raum*

*Berlin-Brandenburg Center for Regenerative Therapies and Berlin-Brandenburg School for Regenerative Therapies, Charité-Universitätsmedizin Berlin, Berlin, Germany; †Department of Applied Physics, University of Eastern Finland, Kuopio, Finland; ‡Department of Biology, Chemistry and Pharmacy, Freie Universität Berlin, Berlin, Germany; §Bioacoustics Research Laboratory, Department of Electrical and Computer Engineering, University of Illinois at Urbana-Champaign, Urbana, Illinois, USA; and ¶Diagnostic Imaging Center, Kuopio University Hospital, Kuopio, Finland

(*Received* 9 *June* 2015; *revised* 24 *January* 2016; *in final form* 27 *January* 2016)

Abstract—Apparent integrated backscatter (*AIB*) is a common ultrasound parameter used to assess cartilage matrix degeneration. However, the specific contributions of chondrocytes, proteoglycan and collagen to *AIB* remain unknown. To reveal these relationships, this work examined biopsies and cross sections of human, ovine and bovine cartilage with 40-MHz ultrasound biomicroscopy. Site-matched estimates of collagen concentration, proteoglycan concentration, collagen orientation and cell number density were employed in quasi-least-squares linear regression analyses to model *AIB*. A positive correlation ($R^2 = 0.51$, $p < 10^{-4}$) between *AIB* and a combination model of cell number density and collagen concentration was obtained for collagen orientations approximately perpendicular (>70°) to the sound beam direction. These findings indicate causal relationships between *AIB* and cartilage structural parameters and could aid in more sophisticated future interpretations of ultrasound backscatter. (E-mail: kay.raum@charite.de) © **2016 World Federation for Ultrasound in Medicine & Biology.**

Key Words: **Apparent integrated backscatter, Cartilage, Ultrasound, Osteoarthritis, Backscatter, Ultrasound spectroscopy, Quantitative ultrasound, Backscatter coefficient.**

INTRODUCTION

Hyaline cartilage is a connective tissue covering the joint surfaces and mediates both friction of adjacent joints and shock absorption. In addition to water, the principal constituents of the cartilage matrix are collagen, proteoglycans and chondrocytes, which are organized heterogeneously with respect to quantity, size and orientation in an arcade-shaped depth-dependent structure (Männicke et al. 2014a). Osteoarthritis (OA) is a joint disease with high socioeconomic impact resulting in a decrease in quality-adjusted life years (Pinto et al. 2012). OA is characterized by progressive degenerative changes in cartilage structure and matrix, chondrocytes and subchondral bone (Buckwalter and Mankin 1998). The first signs of OA are fibrillation or disruption of the superficial cartilage layers, leading to tissue softening and increased surface roughness. Degeneration of the cartilage matrix is characterized by a loss of proteoglycans (aggrecans), followed by a disruption of the collagen network in later stages. To date, none of the established non-invasive imaging modalities are able to assess these degenerative tissue alterations concurrently. The diagnosis of early OA, in particular, is highly important, as it could aid in the development of treatment strategies that aim to arrest or revert the disease progression at an early stage (Chu et al. 2014).

Ultrasound biomicroscopy refers to high-frequency ultrasonic imaging of biological tissues and cells (typically with frequencies >20 MHz), which is capable of visualizing cartilage tissue. The fine spatial resolution on the order of 50–100 μm (Gelse et al. 2010) gives access to a variety of quantitative parameters via temporal separation of the received signals. The most common ultrasound parameters are surface reflection amplitude and surface roughness as surrogates for alterations of cartilage matrix stiffness and surface roughness, respectively. These parameters have been found to significantly vary in

Address correspondence to: Kay Raum, Berlin-Brandenburg School for Regenerative Therapies, Charité-Universitätsmedizin Berlin, Augustenburger Platz 1, 13353 Berlin, Germany. E-mail: kay.raum@charite.de

the course of OA (Kaleva et al. 2008; Nieminen et al. 2009; Saarakkala et al. 2011; Wang et al. 2010) and have been associated with collagen depletion (Nieminen et al. 2002; Töyräs et al. 1999; Wang et al. 2010), surface fibrillation (Saarakkala et al. 2004; Schöne et al. 2013) and biomechanical competence (Gelse et al. 2010; Töyräs et al. 1999) of the tissue. In addition to changes detectable at the cartilage surface, the reflection intensity at the subchondral bone boundary was reported to increase in osteoarthritic samples (Jaffre et al. 2003; Saarakkala et al. 2006). This increase was related to increased bone density and trabecular thickness in the subchondral bone tissue *in vitro* (Liukkonen et al. 2013). Moreover, a degeneration-related decrease in acoustic attenuation of the cartilage matrix was hypothesized to significantly increase the intensity of the subchondral bone reflection (Saarakkala et al. 2011).

Relating the analysis of backscattered ultrasound signals originating from the cartilage matrix to osteoarthritic changes was proposed 20 years ago (Cherin et al. 1998; Kim et al. 1995). The conventional parameter chosen to assess these changes is the apparent integrated backscatter (*AIB*), which quantifies the average backscattered energy within the frequency bandwidth of the transducer. Findings suggest that alterations in collagen packing density and collagen orientation may influence *AIB*. In particular, (i) a decrease in *AIB* with aging in a Wistar rat animal model (Cherin et al. 2001) and (ii) an increase in *AIB* for repair cartilage compared with intact cartilage tissue (Gelse et al. 2010; Laasanen et al. 2006; Viren et al. 2010) were reported. In other work, a decrease in *AIB* was observed after acute impact injury (Viren et al. 2012), whereas a weak but statistically significant increase was reported after enzymatic depletion of collagen and proteoglycans using collagenase and trypsin, respectively (Wang et al. 2010). In contrast, Pellaumail et al. (2002) reported no statistically significant differences in *AIB* after trypsin treatment. However, a direct comparison of these results is difficult, as the frequency ranges used for the calculation of *AIB* varied between studies.

In a recent study, we found that quantitative ultrasound parameters based on envelope statistics and the frequency-dependent spectral slope are more sensitive to degeneration stages of human cartilage than conventionally applied integrated backscatter amplitude parameters (Männicke et al. 2014a). Moreover, in a classification approach using ultrasound based parameter pairs as predictors for cartilage degeneration, we found that parameters of the envelope statistics are feature candidates throughout all degeneration stages, whereas integrated backscatter amplitude and spectral slope appeared to be particularly good predictors for advanced and early stages of degeneration, respectively (Männicke et al. 2014b).

Nevertheless, the diagnostic value of quantitative ultrasound parameters in assessment of cartilage degeneration is limited as long as structural sources giving rise to the backscattered signal remain unknown. Collagen concentration and chondrocyte number density were reported to increase backscatter amplitude in agarose gels (Inkinen et al. 2014) and collagen hydrogels (Mercado et al. 2014; Mercado et al. 2015), strengthening the hypothesis that both the extracellular collagen matrix and chondrocytes contribute to ultrasound backscatter (Männicke et al. 2014a). However, the specific contributions of collagen and cells to backscattered signals have not been clarified for the naturally occurring concentration, composition and orientation of collagen and cells in hyaline cartilage. Therefore, the aims of this study were to characterize hyaline cartilage of different species and to apply species-independent regression models to elucidate causal relationships between ultrasonic backscatter signals measured in the frequency range between 30 and 50 MHz with underlying chemical and structural parameters.

METHODS

Samples

Cartilage specimens were obtained from patellas of human ($N = 16$), bovine ($N = 8$) and ovine ($N = 10$) origin. Human samples were acquired from both left and right lower limbs of human cadavers at the Institute of Anatomy in Lübeck, Germany ($N = 12$) and the Central Finland Central Hospital in Jyväskylä, Finland ($N = 4$). The donor ages were in the range 24–92 years (mean ± standard deviation: 70 ± 20 years). All bovine and four ovine samples were acquired from local abbatoirs (Väisäsen Kotiliha Oy, Iisalmi, Finland, and HKScan Oyj, Outokumpu, Finland, respectively) at estimated animal ages of 1–3 years. Moreover, six ovine specimens were obtained from elderly sheep (4–8 years). At the given animal age ranges, full maturation of human, bovine and ovine cartilage samples was expected. Approval for the experiments was granted from the ethics commissions and approved by local institutional review boards.

Prior to experiments, patellas were stored at −20°C for at least 48 h and up to 10 years (human samples). Using a hollow-core drill (Biltema, Helsingborg, Sweden, diameter = 10 mm), osteochondral cylinders were drilled from the central part of the lateral patella facet. The biopsies comprised the full thickness of cartilage and at least 2 mm of subchondral bone. Immediately after explantation, scalpel cuts at the proximal, medial and lateral sites were set to indicate the anatomical

orientation and enable site matching in later-stage analyses. During drilling, the specimens were rinsed with phosphate-buffered saline (PBS) to reduce excessive heating at biopsy borders. The PBS solution contained inhibitors of proteolytic enzymes, ethylenediaminetetraacetic acid (EDTA, VWR International, Radnor, PA, USA) and benzamide HCl (Sigma-Aldrich, St. Louis, MO, USA), to prevent enzymatic degradation during the experiments and was identical for all successive experimental steps.

After ultrasonic scanning of the intact biopsies, one cross section was prepared for each biopsy along the medial-lateral direction, as indicated by the scalpel markers (Fig. 1a). For this purpose, the sample was fixed at the proximal side. With a precision sectioning saw (IsoMet Low speed saw, Buehler, Lake Bluff, IL, USA), two successive cuts were made, splitting the biopsy into two half-cylinders and one 750-μm-thick cross section (Fig. 1b). The cross sections were marked on the lateral side by cutting off a small piece of bone tissue. The proximal half-cylinder was immediately frozen at -20°C and stored for later need, whereas the distal half-cylinder was fixed in 10% formalin. Subsequently, the formalin-fixed half-cylinder was decalcified with EDTA for 10–14 days and dehydrated in an increasing series of ethanol solutions (80%, 90%, 95%, abs., abs., abs., abs., abs.). Samples were then immersed in molten paraffin wax (Tissue-Tek, Sakura Finetek, Torrance, CA, USA), and several serial cross sections (thickness = 5 μm) were prepared using a microtome (LKB 2218 HistoRange microtome, LKB Produkter, Bromma, Sweden).

Ultrasound

A custom scanning acoustic microscope (BBC Research Group, Kuopio, Finland) was used, consisting of a temperature-controlled tank, a 3-D high-precision scanning stage (T-LSQ, Zaber Technologies, Vancouver, BC, Canada), a 500-MHz dual pulser/receiver (DPR500, JSR Ultrasonics, Pittsford, NY, USA) and a 1.1 GSs-1 A/D card (ADQ112, Signal Processing Devices Sweden, Linköping, Sweden). All components were controlled by custom-developed software written in LabView (LabView 2010, Version 10.0, National Instruments, Austin, TX, USA). The microscope was equipped with one 40-MHz LiNb transducer (NIH Resource Center for Ultrasound Transducer Technology, Los Angeles, CA, USA) and pulse excited using a remote pulser (H2, JSR Ultrasonics). Resulting bandwidths, pulse lengths and focal beam specifications are listed in Table 1. All samples were measured in time-resolved C-scan mode with lateral x- and y-increments of 0.04 mm. The transducer–sample distance was adjusted such that the transducer focus was approximately 0.5 mm below the cartilage surface in the middle of the sample.

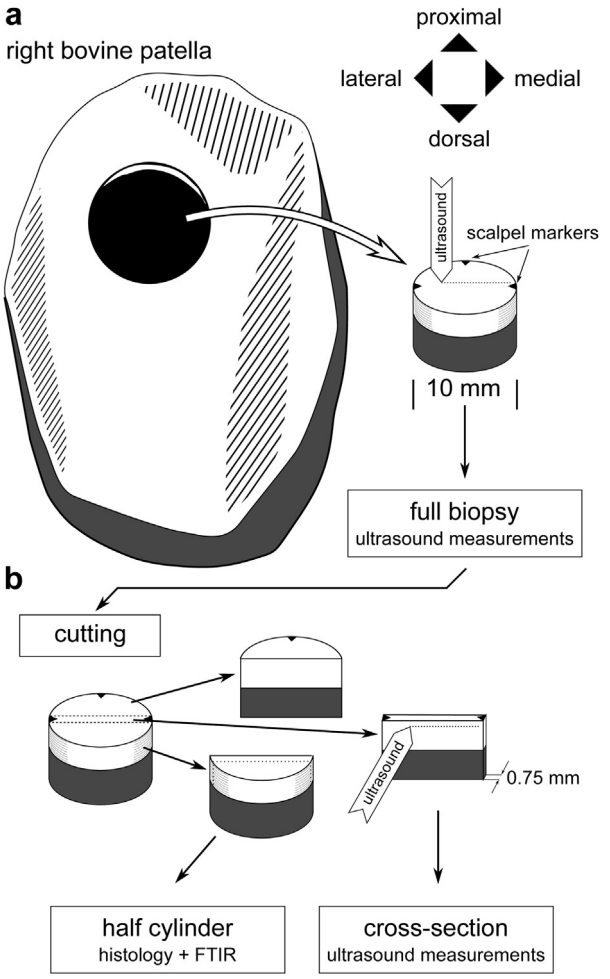

Fig. 1. Main sample processing steps. (a) Biopsy location within the patella with respect to anatomical orientation. Three scalpel markers were placed to preserve the anatomical orientation and to mark the cutting planes for the cross-sectional analyses. Full biopsy ultrasound measurements of the entire cylinder were performed prior to sample cutting. (b) Sample processing steps of the biopsy cylinder. Ultrasound measurements were performed on the obtained cross section, whereas the dorsal half-cylinder was used for light microscopy and Fourier transform infrared imaging spectroscopy (FTIRIS).

Ultrasound measurements of intact full biopsies

Cartilage biopsies were immersed in degassed PBS at 37°C and aligned such that the center of the cartilage surface was oriented perpendicular to the beam axis. Samples were placed in the PBS bath for at least 20 min prior to the start of the experiments to allow adjustment of the sample to the change in temperature in the PBS bath. Samples were positioned such that the proximal side of the biopsy was at the top (Fig. 1a).

Ultrasound measurements of cross sections

The 0.75-mm cross sections were immersed in PBS at 37°C and scanned similarly to the intact samples,

Table 1. Acoustical and geometric properties of the transducer used

Element diameter	3.00 mm
f-Number	2.9
Center frequency*	40.3 MHz
−6-dB bandwidth*	28.2–51.0 MHz
Pulse duration, $\tau(-20\ \mathrm{dB})^{\dagger}$	100 ns
Focal distance‡	8.7 mm
−6-dB focal range‡	6.9–10.4 mm
−6-dB focal beam width	120 μm

* Derived from planar reflector reference measurements.
† Defined as the duration between the times when the pulse amplitude of the confocal echo from a planar reflector is at −20 dB of its maximum value.
‡ Derived from agar–graphite reference measurements.

except that the sound propagation direction for these measurements was perpendicular to the cross-section plane (Fig. 1b). To avoid sample movements during the scans, the cross sections were fixed on a histology slide made of polymethylmethacrylate (PMMA) using two nylon wires (diameter = 90 μm). The wires were placed above the sample and oriented perpendicular to the cartilage surface. Samples were positioned such that the lateral side of the cross section was on the left-hand side.

Data analysis

Definition of regions of interest. To enable a site-matched analysis between measurements in intact full biopsies and in cross sections, the analysis of the full biopsy measurement should comprise only waveforms at locations close to the cross-section position. Therefore, the lateral region of interest (ROI) for the analysis of the full biopsy was composed of multiple circular ROIs with a radius of 0.5 mm along one line, with 50% overlap from medial to lateral scalpel cuts. In Figure 2a, the estimated cross-section position and the corresponding lateral ROIs are indicated in *green* and *white*, respectively. The line was drawn manually in the top-view backscatter amplitude integral (*BAI*) image (Raum et al. 1998) such that scalpel cuts at medial and lateral biopsy ends were not included in the analysis.

For analysis of the cross sections, 15 ROIs were chosen to study the changes of ultrasound parameters with cartilage depth. To define ROI locations, the cartilage surface and subchondral bone boundary were drawn manually in the backscatter amplitude integral image, and 15 equidistant lateral ROIs were defined (Fig. 2c). All areas corresponding to the wires holding the sample were excluded from the analysis. To avoid artifacts close to the subchondral bone interface, the 15th zone—that is, the zone directly adjacent to the subchondral bone boundary—was excluded from all analyses.

Spectral analysis. The backscatter power spectra $|S(f,x,y,z)|^2$ at transducer gate distance z and the lateral

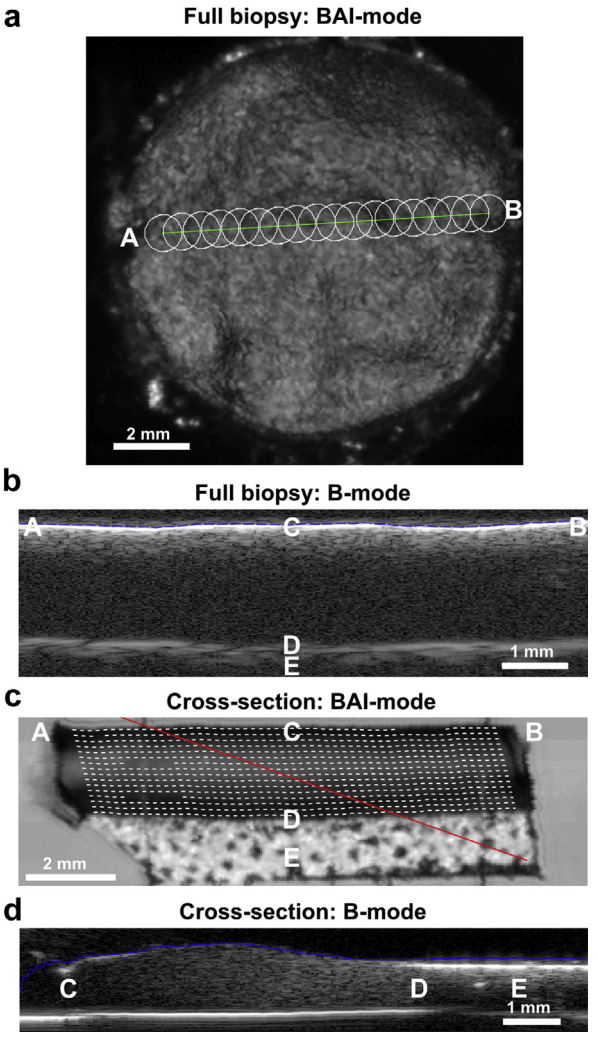

Fig. 2. Ultrasound measurements of a representative bovine sample in full biopsy (a, b) and cross-section (c, d) measurements. (a) Full-biopsy top-view image of the backscattered amplitude integral (*BAI*). (b) Corresponding cross-sectional B-mode image along the line indicated in *green*. (c) Top-view *BAI* image of the sample cross section. The *dashed lines* correspond to the region of interest borders. (d) Corresponding cross-sectional B-mode image along the line indicated in *red*. Letters denote the respective anatomical locations: A and B = start and end of cross section, corresponding to lateral and medial directions, respectively, C = cartilage surface, D = cartilage–subchondral bone interface, E = subchondral bone. All images are scaled equally in both directions.

position (x, y) were estimated by calculating the magnitude squared of the fast Fourier transform of Hamming-windowed time signals. No filtering was applied, but each time-gated signal was zero-padded to a length of 4096 sample points after time gating. A short gate duration of 2.0 pulse lengths (PLs), corresponding to 0.2 μs, was chosen to estimate $|S(f,x,y,z)|^2$. The short gate duration was necessary to avoid averaging artifacts

from rapid tissue changes along the cartilage depth (Männicke et al. 2014a).

The reference spectra, $S_{\mathrm{ref}}(f, z)$, were derived by a combination of one reference scan of a planar PMMA block and one reference scan of a scattering agar–graphite phantom (Männicke et al. 2014a). The planar reflector measurement yields the calibration spectrum $\left|S_{\mathrm{ref}}(f, z_0)\right|$ at the focus z_0. Spectra derived from the scattering phantom, $S_{\mathrm{graphite}}(f, z)$, were normalized to the focus and used to correct for both defocus amplitude decrease and diffraction effects. The reference spectra can then be expressed as

$$S_{\mathrm{ref}}(f,z) = \frac{S_{\mathrm{ref}}(f,z_0)}{R_{\mathrm{PMMA}}} \cdot \frac{S_{\mathrm{graphite}}(f,z)}{S_{\mathrm{graphite}}(f,z_0)} \tag{1}$$

where $R_{\mathrm{PMMA}} = 0.281$ is the reflection coefficient of PMMA. Hence, defocus amplitude and frequency-dependent changes are accounted for by the agar–graphite sample, whereas the overall amplitude is corrected for by the planar reference sample.

The apparent integrated backscatter *AIB*, as given by Cherin et al. (1998), quantifies the backscattered energy within the −6-dB frequency bandwidth Δf

$$AIB(z_s) = \frac{1}{N_{x,y} \cdot \Delta f} \sum\nolimits_{x,y}^{N_{x,y}} \sum_{\Delta f} 10 \cdot \log \left\langle \frac{\left|S(f,x,y,z)\right|^2}{\left|S_{\mathrm{ref}}\ (f,z)\right|^2} \right\rangle \tag{2}$$

whereas $N_{x,y}$ is the number of averaged waveforms. *AIB* was calculated as a function of tissue depth z_s using a sliding window technique (Gelse et al. 2010; Männicke et al. 2014a). In this study, only the maximum value AIB_{max} was of interest, and because of the rapid decrease in backscatter amplitude in cartilage tissue versus depth, the maximum gate depth was set to only 0.3 mm. The first window was centered at the surface position, and an overlap of 95% was chosen between adjacent windows. For a strict differentiation between backscattered waveforms and surface reflection, the surface reflection was gated out by adding the inverted signal multiplied with a Tukey window ($\alpha = 0.5$) at the center position of $z_s = 0$ with a gate length of 2.0 PLs (Männicke et al. 2014a). The conversion from time delays to spatial distances was calculated assuming a constant speed of sound of $c_0 = 1{,}540$ m/s and $c_m = 1{,}620$ m/s for PBS and cartilage tissue (Agemura et al. 1990), respectively.

Light microscopy

The relative proteoglycan and collagen concentrations of the cartilage samples were estimated by Fourier transform infrared imaging spectroscopy (FTIRIS) measurements (Rieppo et al. 2012). Histologic sections were transferred on a 2-mm-thick zinc selenide (ZnSe) window and measured with the FTIR imaging system (Perkin Elmer Spectrum Spotlight 300, Perkin Elmer, Waltham, MA, USA). Measurements were performed in transmission mode in the 4,000–720 cm^{-1} wavenumber range using a spectral resolution of 4 cm^{-1}. A 500-μm-wide area of smooth and intact cartilage was measured from cartilage surface to subchondral bone boundary. The spatial pixel resolution was 25 μm. Three repeated scans were performed and averaged for each specimen. Collagen (Col) and proteoglycan (PG) concentrations were estimated by integration of the amide I region (1,740–1,585 cm^{-1}) and carbohydrate region (1,140–984 cm^{-1}), respectively. Cartilage surface and subchondral bone boundary were selected manually in each scan. Similar to the analysis of the ultrasound scans of the cross sections, the cartilage tissue was divided into 15 equally sized regions with increasing distance to the cartilage surface. In each depth region, average values of proteoglycan and collagen concentration were calculated.

The spatial collagen orientation in cartilage samples was estimated by polarized light microscopy using the polarization microscope Ortholox II POL (Leitz, Wetzlar, Germany) equipped with a camera (Photometrics CH 250/A, Photometrics, Tucson, AZ, USA). Stokes parameters were estimated at 0°, 45° and 90° polarizer pair positions to derive collagen fibril orientation (Rieppo et al. 2008). In accordance with the aforementioned analyses, the average orientation was assessed in 15 depth-dependent zones. Values for 0° and 90° denote collagen fiber orientations parallel and perpendicular to the cartilage surface, respectively.

For each specimen, one histologic section was stained with Safranin O and imaged with a light microscope (Axio Imager M2, Carl Zeiss MicroImaging, Jena, Germany). From the resulting images, the cells were segmented using a threshold-based method followed by morphologic operations and connected component analysis. Because of the gradual increase in Safranin O stain with depth, the cartilage was segmented in six rectangular depth regions. For each region a local threshold was applied, and false detected areas were manually excluded from the cell analysis. The labeled image was cropped to a constant image width of 1 mm and to a non-constant image height depending on the cartilage thickness. Finally, the same depth-dependent analysis was performed; that is, the cartilage surface and subchondral bone boundary were drawn manually and 15 depth-dependent ROIs were analyzed. Within every ROI, the number of connected objects (*i.e.*, chondrocytes) was assessed and normalized by the ROI area, yielding 15 depth-dependent cell number densities (CNDs) in units of mm^{-2} for every sample.

Statistics

One-way analyses of variance followed by *post hoc* Tukey multiple comparison tests were carried out to assess differences in the backscatter amplitudes with respect to the different species. Student's *t*-test was used to assess differences in all evaluated parameters between young and old ovine samples.

Changes in collagen orientation are known to result in changes in ultrasound backscatter intensity (Feltovich et al. 2010) and collagen concentration (Xia et al. 2011). To reduce the potential effect of collagen orientation on the relation between backscatter intensity and collagen concentration, only regions with values larger than 70° with respect to the ultrasound propagation direction (*i.e.*, the average collagen orientation was mostly perpendicular to the ultrasound beam axis) were incorporated into regression models.

Regression models were calculated to predict AIB_{max} estimates obtained from cross-sectional measurements. One-dimensional non-linear regression models were calculated with cell number density, proteoglycan and collagen concentration as predictor variables. Multivariate regression was carried out by quasi-least-squares regressions (Shults and Hilbe 2014) of the GEEQBOX (Ratcliffe and Shults 2008) toolbox using combinations of all three linearized predictor variables. This model accounts for intra-individual correlations of values from the same cross section and used a normally distributed target variable and a Markov correlation structure; that is, adjacent regions of interest are assumed to exhibit a higher correlation than non-adjacent regions. *p*-Values, intercepts and regression coefficients are provided for the individual predictor variables as well as the 95% confidence interval. Moreover, partial and semi-partial correlation coefficients were derived. The goodness of the regression model was analyzed with the Pearson correlation coefficient. Results were considered statistically significant at $p < 0.05$.

RESULTS

Figure 2(a, b) provides representative full biopsy ultrasound images of a bovine sample. Note the characteristic backscatter pattern with high backscatter amplitudes close to the cartilage surface and quick diminishment with cartilage tissue depth (Fig. 2b, C–D direction). In contrast to full biopsy measurements, two major differences can be observed in the cross-sectional images (Fig. 2c, d). First, the backscatter amplitude did not decrease rapidly along the sound propagation direction. Second, the backscatter amplitude gradually increased from the superficial cartilage zone (*C*) toward the cartilage–bone interface (*D*).

Structural parameters

The average collagen orientation obtained by polarized light microscopy was similar for the different species and exhibited the typical changes of collagen orientation from parallel to the cartilage surface in the superficial zone toward perpendicular in deep zones (Fig. 3a). The superficial zone was relatively thin for all samples, as determined by orientations smaller than 50°, highlighting that the zonal organization of the samples was composed of a large (>65%) radial zone and small superficial and tangential (<35%) zones. The cell number density derived from the Safranin O-stained sections was highest and lowest for ovine and human cartilage tissue, respectively (Fig. 3b). A slight decrease from the superficial to the radial zone was observed. FTIR measurements revealed that the concentration of collagen (Fig. 3c) increased non-linearly with cartilage depth for all species. The depth-dependent variation in PG was more complex (Fig. 3d). In the ovine specimens, PG values increased from the central part toward the subchondral bone boundary, whereas in bovine and human cartilage, this increase appeared only in the deeper tissue regions. However, it should be noted that the absolute cartilage thickness in the ovine samples (1.06 ± 0.65 mm) was approximately half of that in the bovine samples (2.08 ± 0.42 mm) and a third of that in human samples (2.94 ± 1.13 mm). Therefore, the absolute thickness of the PG-rich deep cartilage zone was similar for the different species.

Ultrasound parameters

In full biopsy measurements, significantly higher AIB_{max} values were observed for human tissue than for ovine tissue (Fig. 4a). In cross-section measurements, the average backscatter amplitudes in areas with average collagen orientations >70° (*i.e.,* deep cartilage) did not significantly differ between the species (Fig. 4b). However, AIB_{max} was significantly lower in old sheep samples than in young sheep samples. Aged tissue samples also exhibited lower collagen concentrations and cell number densities (Table 2).

Regression analyses

Of the total 510 cross-section measurement ROIs, 225 exhibited a collagen orientation >70° and were included in the regression analyses to predict ultrasound backscatter amplitude in the cross-section measurements.

In the 1-D regression analysis, estimates of collagen concentration ($R^2 = 0.40$, $p < 10^{-4}$) (Fig. 5a), PG concentration ($R^2 = 0.20$, $p < 10^{-4}$, data not shown) and cell number density ($R^2 = 0.41$, $p < 10^{-4}$) (Fig. 5b) exhibited significant correlations with AIB_{max}. The best correlations of collagen and PG concentrations with AIB_{max} were obtained for second-order polynomials

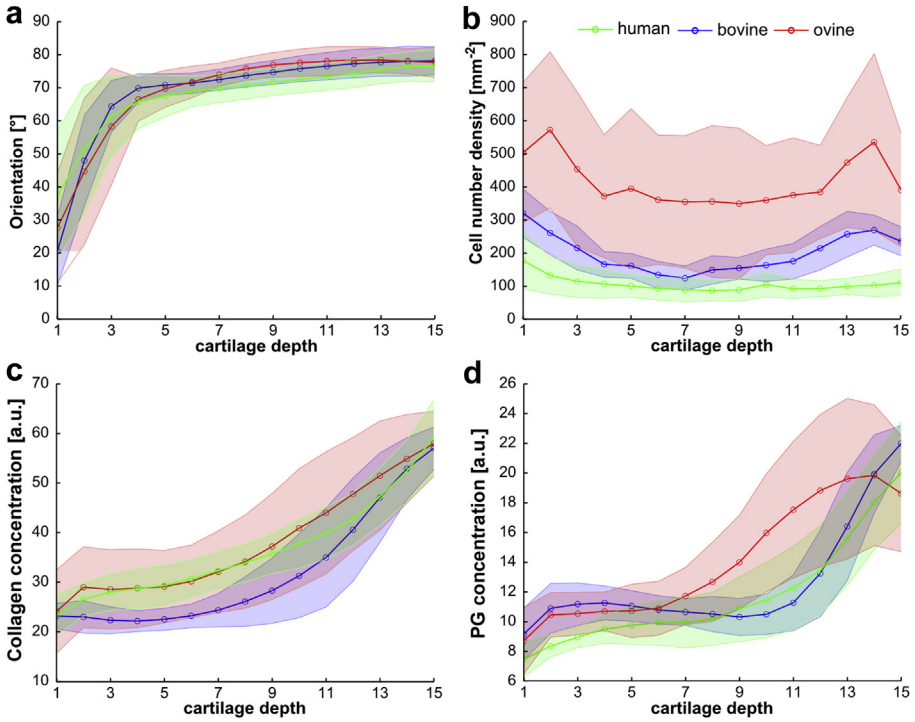

Fig. 3. Average depth-dependent structural and compositional properties for the different species (1 = cartilage surface, 15 = subchondral bone boundary). (a) Average collagen orientation as derived by polarized light microscopy. (b) Average, depth-dependent cell number density. (c) Average collagen concentration (amide I absorbance) as derived by Fourier transform infrared imaging spectroscopy. (d) Average proteoglycan concentration (carbohydrate absorbance) as derived by Fourier transform infrared imaging spectroscopy.

(Fig. 5a), whereas the asymptotic relation between cell number density and $AIB_{\max}$ was best approximated by an exponential model with a decay factor of 0.8. Moreover, a high linear correlation was observed between collagen and PG concentrations ($R^2 = 0.67$, $p < 10^{-4}$) (data not shown).

A quasi-least-squares model for prediction of the $AIB_{\max}$ with linearized collagen concentration, PG concentration and cell number density values as predictor variables resulted in a non-significant contribution of PG to the model. Hence, only the combination of linearized collagen concentration and cell number density values was used (Fig. 5c and Table 3):

$$AIB_{\max} = B_0 + B_{\mathrm{Col}} \cdot \mathrm{Col}^2 + B_{\mathrm{CND}} \cdot \mathrm{CND}^{0.8} \qquad (3)$$

In this model, the exponents for the linearization of Col and CND values were taken from the non-linear regression analysis (Fig. 5a, b). Both regression

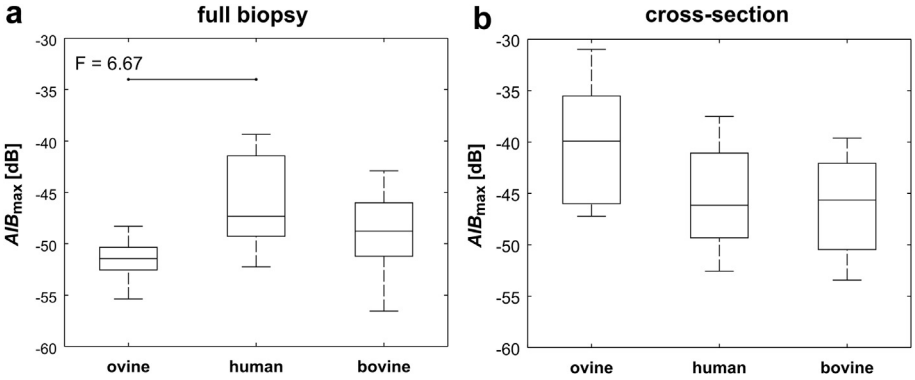

Fig. 4. Boxplots of the maximum backscatter amplitude with respect to the different species for (a) full biopsy and (b) cross-sectional measurements. A significant difference was observed between ovine and human specimens in the full biopsy measurements.

Table 2. Estimated parameters for the two groups of sheep used in this study

	Young sheep	Old sheep
Age	≤3 y	≥4 y
AIB_{max} (dB)	−37.0 ± 2.0	−44.2 ± 3.0*
Collagen concentration (a.u.)	44.3 ± 4.4	35.2 ± 8.7*
Proteoglycan concentration (a.u.)	14.0 ± 2.7	14.6 ± 2.2
Cell number density (mm^{-2})	613 ± 78	307 ± 70*

AIB = apparent integrated backscatter.
* Significant differences (unpaired *t*-test, $p < 0.05$).

coefficients B_{Col} and B_{CND} were positive, indicating that AIB_{max} increased with increasing cell number density and collagen concentration. The partial correlation coefficients suggest an approximately equal impact of Col and CND variations on the explained variation of AIB_{max}. As derived by the squared semi-partial correlation coefficients, 18% and 20% of the total variation of AIB_{max} could be attributed to Col and CND, respectively.

DISCUSSION

In this study, we analyzed the apparent integrated backscatter (AIB_{max}) in hyaline cartilage tissue in different species with respect to chemical composition and collagen orientation. A moderate correlation between collagen concentration and ultrasound backscatter amplitude was observed for regions with a collagen orientation approximately perpendicular (>70°) to the sound beam direction. This is in agreement with several previous studies that proposed an impact of collagen concentration on ultrasound backscatter (Bridal et al. 2006; Feltovich et al. 2010; Pohlhammer and O'Brien 1981). In the current study, we found that under the aforementioned conditions, approximately 18% of the total variation in AIB_{max} could be attributed to the collagen concentration variation.

Table 3. Non-linear quasi-least-squares regression model used to predict AIB_{max} with collagen concentration and cell number density as predictor variables (eqn 3)*

	B_0 (dB)	B_{Col} (dB)	B_{CND} (dB·mm^2)
B_i	−52.86	$3.8e^{-3}$	$1.7e^{-2}$
Z	—	11.10	2.59
Partial correlation	—	0.56	0.58
Semipartial correlation	—	0.43	0.45
p	—	$<10^{-4}$	$<10^{-3}$

AIB = apparent integrated backscatter.
* Absolute coefficients B_i, z-statistics value z, partial and semipartial correlation coefficients, and p-values for the individual parameters ($N = 252$, $R^2 = 0.51$, $p < 10^{-4}$, RMSE = 2.7 dB).

In addition to collagen concentration, a statistically significant positive correlation of cell number density and AIB_{max} was observed. This finding is in agreement with a previously reported moderate univariate correlation ($R^2 = 0.43$) observed in human cartilage with variable degrees of degeneration (Männicke et al. 2014a).

Using collagen concentration and cell number density, we found that a 2-D regression model can account for approximately 50% of the observed variation in ultrasound backscatter. This finding is in line with previous reports suggesting that both chondrocytes and collagen contribute to ultrasound backscatter in this frequency range. However, the following reasons do not allow extension of the proposed model derived from cross-section measurements to full biopsy measurements. First, deep zones of cartilage cross sections with relatively large and round-shaped chondrocytes were used for development of the backscatter model. This model is probably biased in predictions of backscatter from smaller chondrocytes with elliptical shape, corresponding to cells in the superficial zone in measurements through the cartilage surface. Second, we observed that in contrast to ovine and bovine specimens, human tissue exhibited significantly higher backscatter amplitudes in

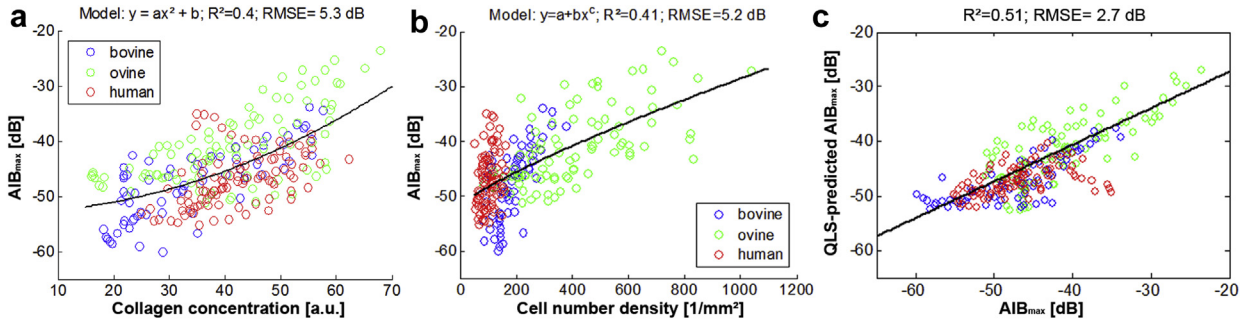

Fig. 5. Non-linear regression models with AIB_{max} as target variable and (a) collagen concentration (amide I absorbance) and (b) cell number density as predictor variables. Suitable linearization was approximated by polynomial models with growth and decay factors of 2 and 0.8 for collagen concentration and cell number density, respectively. (c) Multivariate model with linearized collagen concentration and cell number density as predictor variables for AIB_{max}.

the full biopsy measurements. The latter could not be explained by the number of cells and amount of collagen in the superficial zone of human tissue, which were not higher compared with those of ovine or bovine specimens. This apparent deviation of predicted and measured backscatter amplitudes in human cartilage must be attributed to other factors than collagen or cell number density.

Human tissue exhibited mild signs of degeneration because the somewhat high donor ages and the observation of almost isotropic backscatter characteristics led to two different hypotheses. On the one hand, cartilage degeneration results in tissue softening and subsequently leads to a reduction in the reflection coefficient. Therefore, more sound energy is transmitted into the tissue matrix and can be scattered at subsurface scatterers. A degeneration-related reduction of acoustic attenuation (Nieminen et al. 2004) contributes to this effect. This hypothesis is supported by Wang et al. (2010), who reported a statistically significant increase in backscatter amplitude in the middle cartilage zone after enzymatic digestion with trypsin or collagenase. On the other hand, fibrillation of the superficial cartilage zone in the course of cartilage degeneration introduces additional acoustic impedance interfaces within the tissue that can contribute to the detected ultrasound backscatter amplitude in human tissue, as reported by Myers et al. (1995), who observed a significant correlation between the width of the surface echo band (corresponding to the subsurface backscatter signals analyzed in this study) and cartilage fibrillation depth. Considering the small depth of the gating window of approximately 160 μm, probably both effects contribute to increased backscatter amplitudes in human samples. However, the observation of increased backscatter amplitude in degenerated cartilage is in contrast to a previous finding of no statistical differences in AIB_{max} with respect to early degeneration grades (Männicke et al. 2014a).

The following limitations of this study should be mentioned. Intra- and inter-specimen differences in swelling behavior of cartilage cross sections may result in underestimated backscatter amplitudes in cross-section measurements because of increased water content and a subsequent decrease in scatterer number density. Moreover, the swelling-associated surface inclination may result in heterogeneous acoustic pressure amplitudes of the cross-section areas. Another experimental limitation is related to the sample origin. In contrast to human and bovine cartilage samples with cartilage thicknesses >2 mm, ovine tissue exhibited thicknesses in the range 0.7–1.1 mm. The lower thicknesses caused a decrease in the number of available pulse echoes in the spectra estimation of the cross-section measurements.

CONCLUSIONS

For the first time, we observed a positive correlation between ultrasound backscatter intensity in the frequency range around 40 MHz and cell number density and collagen concentration in hyaline cartilage of different species (human, ovine and bovine). The model yielded a good prediction of the integrated backscatter for all species and tissue ages when the collagen orientation was approximately perpendicular to the sound propagation direction. The variability of collagen concentration had a similar impact on the variation in ultrasound backscatter as variations of cell number density. These findings may aid the future diagnostic potential of ultrasound for cartilage characterization by improved understanding of the backscatter amplitude origins. Future work should aim to apply more sophisticated analyses of spectral features of backscattered ultrasound from the cartilage matrix, such as the spectral slope, as they could serve as a highly sensitive indicator of early OA.

Acknowledgments—This work was supported by the German Research Council (DFG Grant Ra1380/6-1). N.M. received a DFG stipend through the Berlin-Brandenburg School for Regenerative Therapies GSC 203. Research was conducted in the framework of the Baltic Sea Network "Quantitative Imaging of Functional Competence of the Musculoskeletal System" (QUIMUS, Grants 01DS12027 and 01DS13006). K.R. received funding through the BMBF musculoskeletal research network OVERLOAD-PrevOP (subproject SPP6).

REFERENCES

Agemura DH, O'Brien WD Jr, Olerud JE, Chun LE, Eyre DE. Ultrasonic propagation properties of articular cartilage at 100 MHz. J Acoust Soc Am 1990;87:1786–1791.

Bridal SL, Fournier C, Coron A, Leguerney I, Laugier P. Ultrasonic backscatter and attenuation (11–27 MHz) variation with collagen fiber distribution in *ex vivo* human dermis. Ultrason Imaging 2006;28:23–40.

Buckwalter JA, Mankin HJ. Articular cartilage: Degeneration and osteoarthritis, repair, regeneration, and transplantation. Instr Course Lect 1998;47:487–504.

Cherin E, Saied A, Laugier P, Netter P, Berger G. Evaluation of acoustical parameter sensitivity to age-related and osteoarthritic changes in articular cartilage using 50-MHz ultrasound. Ultrasound Med Biol 1998;24:341–354.

Cherin E, Saied A, Pellaumail B, Loeuille D, Laugier P, Gillet P, Netter P, Berger G. Assessment of rat articular cartilage maturation using 50-MHz quantitative ultrasonography. Osteoarthritis Cartilage 2001;9:178–186.

Chu CR, Millis MB, Olson SA. Osteoarthritis: From palliation to prevention: AOA Critical Issues. J Bone Joint Surg Am 2014;96:e130.

Feltovich H, Nam K, Hall TJ. Quantitative ultrasound assessment of cervical microstructure. Ultrason Imaging 2010;32:131–142.

Gelse K, Olk A, Eichhorn S, Swoboda B, Schöne M, Raum K. Quantitative ultrasound biomicroscopy for the analysis of healthy and repair cartilage tissue. Eur Cell Mater 2010;19:58–71.

Inkinen S, Liukkonen J, Ylarinne JH, Puhakka PH, Lammi MJ, Viren T, Jurvelin JS, Töyräs J. Collagen and chondrocyte concentrations control ultrasound scattering in agarose scaffolds. Ultrasound Med Biol 2014;40:2162–2171.

Jaffre B, Watrin A, Loeuille D, Gillet P, Netter P, Laugier P, Saied A. Effects of antiinflammatory drugs on arthritic cartilage: A high-frequency quantitative ultrasound study in rats. Arthritis Rheum 2003;48:1594–1601.

Kaleva E, Saarakkala S, Töyräs J, Nieminen HJ, Jurvelin JS. *In-vitro* comparison of time-domain, frequency-domain and wavelet ultrasound parameters in diagnostics of cartilage degeneration. Ultrasound Med Biol 2008;34:155–159.

Kim HK, Babyn PS, Harasiewicz KA, Gahunia HK, Pritzker KP, Foster FS. Imaging of immature articular cartilage using ultrasound backscatter microscopy at 50 MHz. J Orthop Res 1995;13:963–970.

Laasanen MS, Töyräs J, Vasara A, Saarakkala S, Hyttinen MM, Kiviranta I, Jurvelin JS. Quantitative ultrasound imaging of spontaneous repair of porcine cartilage. Osteoarthritis Cartilage 2006;14: 258–263.

Liukkonen J, Hirvasniemi J, Joukainen A, Penttila P, Viren T, Saarakkala S, Kroger H, Jurvelin JS, Töyräs J. Arthroscopic ultrasound technique for simultaneous quantitative assessment of articular cartilage and subchondral bone: An *in vitro* and *in vivo* feasibility study. Ultrasound Med Biol 2013;39:1460–1468.

Männicke N, Schöne M, Gottwald M, Göbel F, Oelze ML, Raum K. 3-D high-frequency ultrasound backscatter analysis of human articular cartilage. Ultrasound Med Biol 2014a;40:244–257.

Männicke N, Schöne M, Oelze ML, Raum K. Articular cartilage degeneration classification by means of high-frequency ultrasound. Osteoarthritis Cartilage 2014b;22:1577–1582.

Mercado KP, Helguera M, Hocking DC, Dalecki D. Estimating cell concentration in three-dimensional engineered tissues using high frequency quantitative ultrasound. Ann Biomed Eng 2014;42: 1292–1304.

Mercado KP, Helguera M, Hocking DC, Dalecki D. Noninvasive quantitative imaging of collagen microstructure in three-dimensional hydrogels using high-frequency ultrasound. Tissue Eng Part C Methods 2015;21:671–682.

Myers SL, Dines K, Brandt DA, Brandt KD, Albrecht ME. Experimental assessment by high frequency ultrasound of articular cartilage thickness and osteoarthritic changes. J Rheumatol 1995;22:109–116.

Nieminen HJ, Saarakkala S, Laasanen MS, Hirvonen J, Jurvelin JS, Töyräs J. Ultrasound attenuation in normal and spontaneously degenerated articular cartilage. Ultrasound Med Biol 2004;30: 493–500.

Nieminen HJ, Töyräs J, Rieppo J, Nieminen MT, Hirvonen J, Korhonen R, Jurvelin JS. Real-time ultrasound analysis of articular cartilage degradation *in vitro*. Ultrasound Med Biol 2002;28: 519–525.

Nieminen HJ, Zheng Y, Saarakkala S, Wang Q, Töyräs J, Huang Y, Jurvelin JS. Quantitative assessment of articular cartilage using high-frequency ultrasound: Research findings and diagnostic prospects. Crit Rev Biomed Eng 2009;37:461–494.

Pellaumail B, Watrin A, Loeuille D, Netter P, Berger G, Laugier P, Saied A. Effect of articular cartilage proteoglycan depletion on high frequency ultrasound backscatter. Osteoarthritis Cartilage 2002;10:535–541.

Pinto D, Robertson MC, Hansen P, Abbott JH. Cost-effectiveness of nonpharmacologic, nonsurgical interventions for hip and/or knee osteoarthritis: Systematic review. Value Health 2012;15:1–12.

Pohlhammer J, O'Brien WD Jr. Dependence of the ultrasonic scatter coefficient on collagen concentration in mammalian tissues. J Acoust Soc Am 1981;69:283–285.

Ratcliffe SJ, Shults J. GEEQBOX: A MATLAB toolbox for generalized estimating equations and quasi-least squares. J Stat Software 2008; 25:1–14.

Raum K, Ozguler A, Morris SA, O'Brien WD Jr. Channel defect detection in food packages using integrated backscatter ultrasound imaging. IEEE Trans Ultrason Ferroelectr Freq Control 1998;45:30–40.

Rieppo J, Hallikainen J, Jurvelin JS, Kiviranta I, Helminen HJ, Hyttinen MM. Practical considerations in the use of polarized light microscopy in the analysis of the collagen network in articular cartilage. Microsc Res Tech 2008;71:279–287.

Rieppo L, Rieppo J, Jurvelin JS, Saarakkala S. Fourier transform infrared spectroscopic imaging and multivariate regression for prediction of proteoglycan content of articular cartilage. PLoS One 2012;7:e32344.

Saarakkala S, Laasanen MS, Jurvelin JS, Töyräs J. Quantitative ultrasound imaging detects degenerative changes in articular cartilage surface and subchondral bone. Phys Med Biol 2006;51: 5333–5346.

Saarakkala S, Töyräs J, Hirvonen J, Laasanen MS, Lappalainen R, Jurvelin JS. Ultrasonic quantitation of superficial degradation of articular cartilage. Ultrasound Med Biol 2004;30:783–792.

Saarakkala S, Wang SZ, Huang YP, Jurvelin JS, Zheng YP. Characterization of center frequency and bandwidth of broadband ultrasound reflected by the articular cartilage to subchondral bone interface. Ultrasound Med Biol 2011;37:112–121.

Schöne M, Männicke N, Gottwald M, Göbel F, Raum K. 3-D High frequency ultrasound improves the estimation of surface properties in degenerated cartilage. Ultrasound Med Biol 2013;39:834–844.

Shults J, Hilbe JM. Quasi-least squares regression. Boca Raton, FL: CRC Press, 2014.

Töyräs J, Rieppo J, Nieminen MT, Helminen HJ, Jurvelin JS. Characterization of enzymatically induced degradation of articular cartilage using high frequency ultrasound. Phys Med Biol 1999;44: 2723–2733.

Viren T, Saarakkala S, Jurvelin JS, Pulkkinen HJ, Tiitu V, Valonen P, Kiviranta I, Lammi MJ, Töyräs J. Quantitative evaluation of spontaneously and surgically repaired rabbit articular cartilage using intra-articular ultrasound method in situ. Ultrasound Med Biol 2010;36: 833–839.

Viren T, Timonen M, Tyrvainen H, Tiitu V, Jurvelin JS, Töyräs J. Ultrasonic evaluation of acute impact injury of articular cartilage *in vitro*. Osteoarthritis Cartilage 2012;20:719–726.

Wang SZ, Huang YP, Saarakkala S, Zheng YP. Quantitative assessment of articular cartilage with morphologic, acoustic and mechanical properties obtained using high-frequency ultrasound. Ultrasound Med Biol 2010;36:512–527.

Xia Y, Mittelstaedt D, Ramakrishnan N, Szarko M, Bidthanapally A. Depth-dependent anisotropies of amides and sugar in perpendicular and parallel sections of articular cartilage by Fourier transform infrared imaging. Microsc Res Tech 2011;74:122–132.